Eur Radiol (2013) 23:408–416
DOI 10.1007/s00330-012-2614-z

HEPATOBILIARY-PANCREAS

Two- versus three-dimensional dual gradient-echo MRI of the liver: a technical comparison

Michael A. Fischer · Olivio F. Donati · Natalie Chuck · Iris N. Blume · Roger Hunziker · Hatem Alkadhi · Daniel Nanz

Received: 22 February 2012 / Revised: 3 July 2012 / Accepted: 8 July 2012 / Published online: 4 August 2012

Abstract
Objective To compare 2D spoiled dual gradient-echo (SPGR-DE) and 3D SPGR-DE with fat and water separation for the assessment of focal and diffuse fatty infiltration of the liver.
Methods A total of 227 consecutive patients (141 men; 56± 14 years) underwent clinically indicated liver MRI at 1.5 T including multiple-breath-hold 2D SPGR-DE and single-breath-hold 3D SPGR-DE with automatic reconstruction of fat-only images. Two readers assessed the image quality and number of fat-containing liver lesions on 2D and 3D in- and opposed-phase (IP/OP) images. Liver fat content (LFC) was quantified in 138 patients without chronic liver disease from 2D, 3D IP/OP, and 3D fat-only images.
Results Mean durations of 3D and 2D SPGR-DE acquisitions were 23.7±2.9 and 97.2±9.1 s respectively. The quality of all 2D and 3D images was rated diagnostically. Three-dimensional SPGR-DE revealed significantly more breathing artefacts resulting in lower image quality ($P<0.001$); 2D and 3D IP/OP showed a similar detection rate of fat-containing lesions ($P=0.334$) and similar LFC estimations (mean: +0.4 %; $P=0.048$). LFC estimations based on 3D fat-only images showed significantly higher values (mean: 2.7 % + 3.5 %) than those from 2D and 3D IP/OP images ($P<0.001$).
Conclusion Three dimensional SPGR-DE performs as well as 2D SPGR-DE for the assessment of focal and diffuse fatty infiltration of liver parenchyma. The 3D SPGR-DE sequence used was quicker but more susceptible to breathing artefacts. Significantly higher LFC values are derived from 3D fat-only images than from 2D or 3D IP/OP images.

M. A. Fischer (✉) · O. F. Donati · N. Chuck · I. N. Blume · R. Hunziker · H. Alkadhi · D. Nanz
Institute of Diagnostic and Interventional Radiology,
University Hospital Zurich,
Raemistr. 100,
8091 Zurich, Switzerland
e-mail: michaelalexander.fischer@usz.ch

Key Points
- *Magnetic resonance imaging can assess focal and diffuse hepatic fatty infiltration*
- *Both 2D and 3D dual-echo MRI techniques can be used for chemical shift imaging of the liver.*
- *The single breath-hold 3D dual-echo technique is faster but more susceptible to breathing artefacts.*
- *Three-dimensional fat-only images show higher fat estimates than in- and out-of-phase images.*

Keywords Liver fat content · Three-dimensional spoiled gradient echo · Magnetic resonance imaging · In- and opposed-phase imaging · Image quality

Introduction

Hepatosteatosis affects approximately 30 % of adults and 13 % of children in the Western countries [1]. It is a risk factor for the development of liver cirrhosis and hepatocellular carcinoma (HCC) [2] as well as for the development of postoperative complications following liver surgery [3]. Magnetic-resonance dual-echo (DE) and multi-echo (ME) imaging is one of the most accurate and versatile non-invasive tools for assessment of steatosis and fat-containing lesions of the liver [4], challenging liver biopsy as the reference standard for liver fat content (LFC) quantification [5, 6]. Whereas DE-MRI allows for accurate quantification of LFC in patients without elevated liver iron [7–10], ME-MRI sequences are able to correct for the confounding T2* bias introduced by paramagnetic iron depositions [11, 12] coexisting with liver steatosis fat in patients suffering from diffuse liver disease [13].

In routine clinical practice, most standard hepatic MR imaging protocols to date include two gradient-echo acquisitions: (1) 2D dual-echo in- and opposed-phase imaging (2D SPGR-DE) is used to identify diffuse or focal fatty infiltration of the

liver; (2) 3D dynamic, fat-signal-suppressing imaging with baseline and multiple acquisitions following intravenous contrast medium is used for lesion characterisation. Recently, 3D spoiled dual-gradient echo (3D SPGR-DE) sequences were introduced that allow true volumetric acquisition of the entire liver in a single breath-hold. These new sequences allow for reconstruction of water-signal- and fat-signal-only image series and for generation of in- and opposed-phase (IP/OP) images. Preliminary data suggest that the water-only 3D SPGR-DE image series may hold diagnostically competitive information compared to the standard 3D dynamic protocol (2) for dynamic imaging [14]. However, it remains unclear if these 3D sequences could equally replace the 2D IP/OP acquisitions for assessment of liver fat. If so, a single 3D SPGR-DE acquisition could replace both the multiple-breath-hold 2D SPGR-DE and the unenhanced baseline acquisition of the dynamic images, resulting in shorter and more time-efficient liver MR imaging protocols.

The purpose of our study was to evaluate whether a single breath-hold 3D SPGR-DE acquisition could potentially replace standard multiple breath-hold 2D IP/OP acquisitions for the assessment of focal and diffuse fatty infiltration of the liver, and to evaluate benefits from the fat- and water-signal-separating image reconstruction in liver fat quantification.

Material and methods

Patients

Institutional review board approval and a waiver of informed consent were obtained for this study. Between January and August 2010 a total of 227 consecutive patients (141 men; 86 women; mean age 56±14; range 15–84 years) were included. Reasons for referral for liver MR imaging were: screening for metastasis of gastrointestinal malignancy (n=22; 10 %), screening of HCC (n=54; 24 %), primary staging of focal liver lesions detected by CT or ultrasound (n=51; 22 %), re-staging of focal liver lesions after chemo-/radio- or interventional therapy (n=31; 14 %), assessment of the bile-duct system (n=48; 21 %), pre-transplant liver assessment (n =7; 3 %), and assessment of diffuse liver disease including elevated liver iron and steatosis (n=14; 6 %).

Patients (n=88) with histopathologically or image-based proven cirrhosis or haemosiderosis of the liver were excluded from quantitative analysis of LFC as diffuse liver disease is usually associated with mild-to-severe iron overload [13], which is a known confounder of fat quantification by dual-echo MRI (see "Introduction"). Thus, LFC was quantified in a subpopulation of 139 patients (86 men; 55 women; mean age 52±16; range 15–79 years) showing no clinical or image-based signs of diffuse liver disease.

Magnetic resonance imaging

All MR imaging was performed at 1.5 T (Signa Echospeed EXCITE HDxt, GE Healthcare, Waukesha, WI, USA) with patients in supine position using an eight-element body-array coil. Overview and calibration sequences for surface-coil sensitivity were acquired in inspiration. Both the 2D SPGR-DE and the 3D SPGR-DE were performed before contrast agent administration. In order to cover the full liver volume, the 2D SPGR-DE series were acquired in two to four breath-hold periods with the following acquisition parameters: repetition time (TR) (ms)/echo time (TE) (ms), 135/2.2 (OP), 4.6 (IP), flip angle 60°; section thickness 5 mm, inter-slice gap 1 mm, bandwidth ±50 kHz, acquisition matrix 224×192, parallel imaging acceleration factor 2, and acquisition time 14 s/breath-hold.

The 3D SPGR-DE series was planned to cover the entire liver in a single breath-hold with acquisition parameters adjusted to the single-echo 3D GRE unenhanced sequence, which we aimed to replace by the 3D SPGR-DE sequence: TR/TE (ms) 6.3–6.7/3.1–3.2 (echo 1), 6.4–6.5 (echo 2), flip angle 12°, section thickness 4 mm, inter-slice gap 0 mm, bandwidth ± 83.3 kHz, acquisition matrix 256–320×160–224; number of sections 42–74, parallel imaging acceleration factor of 1.7–1.8, and acquisition time 14.4–30.3 s. The 3D SPGR-DE sequence (LAVA FLEX, GE Healthcare, Waukesha, WI, USA) is characterised by a chemical-shift-selective, "Dixon-based" postprocessing algorithm that automatically generates fat- and water-signal-only images in addition to conventional IP/OP images (Fig. 2). Fat- and water-only images are thereby reconstructed after fast Fourier transformation of IP/OP images using a region-growing algorithm that also considers signal phase, as proposed by Ma et al. [15]. The 2D and 3D dual-echo imaging was embedded in the standard liver protocol of our department, which also includes the acquisition of non-enhanced 2D coronal T2-weighted single-shot fast spin-echo images, axial T2-weighted fat-suppressing fast spin-echo images, optional axial fast imaging employing steady-state images, and contrast-enhanced dynamic acquisitions with a T1-weighted 3D spoiled SPGR sequence.

MR image analysis

Images were analysed both qualitatively and quantitatively in three reading sessions with a gap of 2–3 weeks between each session.

The qualitative assessment was performed by two experienced abdominal radiologists (4 and 5 years of experience), who were blinded to clinical findings and to all imaging sequences but 2D and 3D SPGR-DE (reading sessions 1 and 2). The quantitative analysis was performed by a third abdominal radiologist (4 years of experience) who was blinded to the results from qualitative image analysis.

All images were interpreted on a standard workstation (AW 3.2; GE Medical Systems) and were presented to the readers with the minimum of annotations allowed by the software. Prior to the readout, an assembly with examples for types of imaging artefacts created from different images than those from this study was used to train readers in artefact identification to obtain uniform classification.

Reading session 1, qualitative assessment

Two-dimensional and 3D IP/OP SPGR-DE images were reviewed side by side to allow for direct 2D vs. 3D comparison.

Anatomy depiction For liver, kidneys, and adrenal glands, the reviewers compared the depiction of parenchymal details and anatomy, ranking the two types of images according to (1) 2D equal to 3D, (2) 2D better than 3D, or (3) 3D better than 2D. The parameters for anatomical depiction included the assessment of clarity of organ edges and vessels compared to organ parenchyma.

Image artefacts The 2D and 3D IP/OP images were screened for the presence of image artefacts, including ringing artefacts, susceptibility artefacts, blurring and ghosting artefacts caused by physiological, mostly respiratory, motion, inflow artefacts, parallel imaging artefacts, and vascular ghosting artefacts (Fig. 1). Subsequently, the overall artefact levels of 2D and 3D data sets were compared and ranked according to (1) 2D equal to 3D, (2) 2D better than 3D, or (3) 3D better than 2D.

Overall image quality At the end of the first reading session, image quality was graded on a five-point scale: (1) severe artefacts, non-diagnostic image quality; (2) major artefacts, poor but diagnostic image quality; (3) moderate artefacts, fair and diagnostic image quality; (4) few artefacts, good and diagnostic image quality; (5) excellent and diagnostic image quality with no or minimal artefacts.

Reading session 2, detection of liver lesions

All 2D and 3D SPGR-DE images were reviewed separately and in random order to minimise opportunities for direct conscious comparison of 2D versus 3D SPGR-DE images.

Detection of liver lesions The total number of liver lesions (1 to 9, 10 or more) detected in both 2D and 3D IP/OP images was recorded. Additionally, the number of fat-containing lesions (1 to 9, 10 or more) was determined separately (Fig. 2).

Reading session 3, quantitative LFC assessment

For quantitative analysis, 2D and 3D SPGR-DE image series as well as all required fat fraction maps (see below) were simultaneously loaded into the standard volume-viewer software installed on a workstation AW 4.3 (GE Medical Systems), which provided co-registration of all

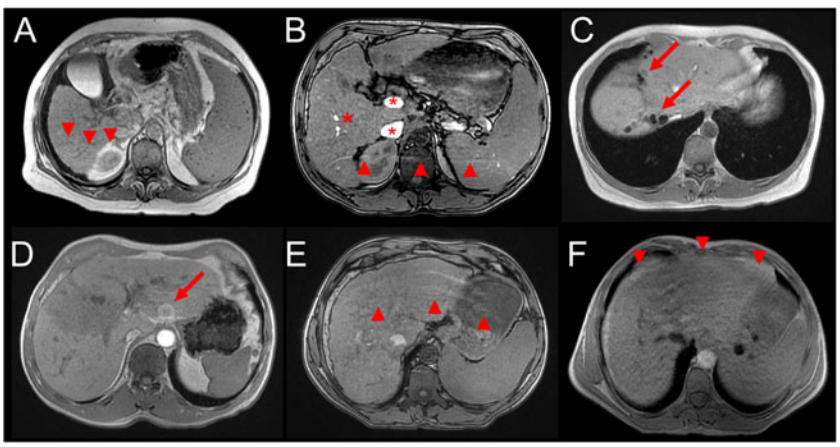

Fig. 1 Axial 2D and 3D IP/OP images showing common artefacts in gradient-echo imaging: **a** Bright lines adjacent to the liver segment VI indicate "Gibbs" or "truncation" artefacts (*arrowheads*) apparent at borders of abrupt intensity change. **b** Hyperintense vessels (*asterix*) indicate "in-flow" artefacts (not thrombosis) due to entry of unsaturated spins into the imaging plane/slice. **b** Bright horizontal line (*arrowheads) in phase-encoding direction indicates "parallel-imaging" artefact.* **c** *Hypointense lesions indicate "susceptibility" artefacts due to postoperative metal clips. (***d–f***) Ghosting artefacts are usually caused by movements (e.g., respiratory motion, arterial pulsations) and appear in the phase-encoding direction. "Vascular ghosting" artefact might simulate an intrahepatic lesion (arrow).* **e** *Motion ghosting artefacts appear as lines (arrowheads) extending across the entire field of view (unlike Gibbs ringing), whereas* **f** *"motion blurring" artefacts are characterised as increased noise (arrowheads) usually seen in fast breathing patients*

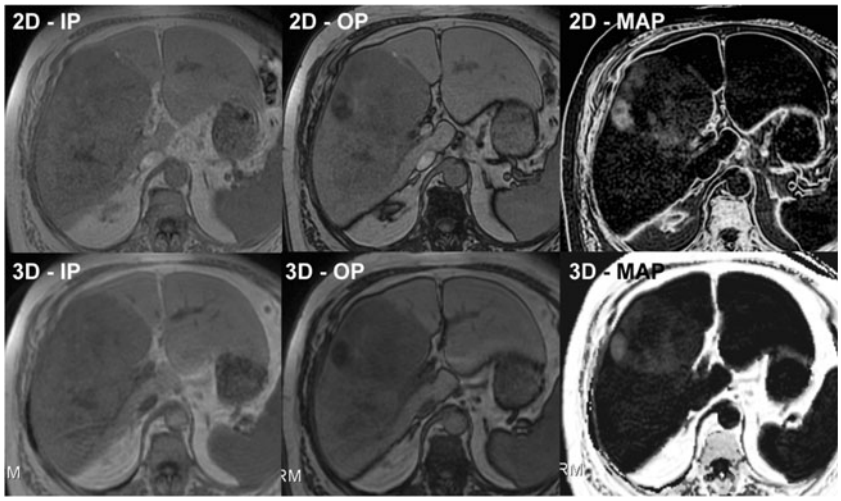

Fig. 2 Axial 2D and 3D IP/OP images with corresponding fat fraction maps of a 76-year-old patient suffering from hepatitis C with a histopathologically proven HCC in a non-cirrhotic liver. Both 2D and 3D OP images show a significant signal drop in the right liver lobe (segment VIII) with corresponding elevated signal intensity on the fat fraction maps consistent with a fat-containing tumour. In this patient both sequences were considered equivalent regarding the detection of focal fatty infiltration

image sets as well as exact matching of the ROIs and VOIs positioned on them.

Liver fat content, LFC For quantification of liver fat, fat signal fractions (FSF) were measured in parametric fat fraction maps derived from 2D and 3D IP and OP and 3D water- and fat-only images, respectively, with software based on "pydicom" [16] and the following formulas:

(1) $FSF_{IP/OP}$ was obtained from both 2D SPGR-DE and 3D SPGR-DE as the signal difference between IP and OP images divided by the doubled IP signal: $FSF_{in/op} = \left|SI_{ip} - SI_{op}\right| / 2SI_{ip}$; where the difference SI_{ip}-SI_{op} was limited to values greater than or equal to zero. The fat- and water-separated images of the 3D data set were used to resolve the ambiguity associated with the magnitude nature of the source (IP and OP) images in the 3D case.
(2) FSF_{FAT} was obtained from the fat-only image (SI_{FAT}) divided by the signal of both the water- (SI_{WATER}) and the fat-only image (SI_{FAT}): $FSF_{FAT} = SI_{FAT} / (SI_{WATER} + SI_{FAT})$.

For each patient, regions of interest (ROI) were placed on the IP image in liver segments II and VIII, as well as into subcutaneous and abdominal fat, avoiding vessels and biliary ducts or areas affected by imaging artefacts. The ROI was automatically co-registered into all loaded image sets, thus enabling fat quantification at the same position on all image and parametric-map series.

Statistical analysis

Variables are reported as mean ± standard deviation or as frequencies and percentages. The data were descriptively reviewed and statistically tested for normality with the Kolmogorov-Smirnov test.

Correlation between 2D and 3D MR imaging measurements as well as correlation between 3D image acquisition times and image quality was assessed using Pearson's correlation analysis. Wilcoxon-signed rank test was used to test for significant differences between qualitative (ordinal variables) MR imaging measurements, whereas the paired samples *t*-test was used for quantitative data (continuous variables).

The inter-observer agreement of qualitative LFC measurements was assessed with *k* statistics and was interpreted as follows: k-value>0.81: excellent agreement, $0.60<k$-value≤ 0.80: very good agreement, $0.40<k$-value≤ 0.60: good agreement, and $0.20<k$-value≤ 0.40: moderate agreement.

P-values <0.05 were considered statistically significant. All statistical analyses were performed using commercially available software (SPSS, release 17.0, Chicago, IL, USA).

Results

A summary of the results from qualitative image analysis is shown in Table 1; a summary of the LFC assessments is provided in Table 2.

Anatomy depiction Both readers rated the general visualisation of the liver, kidneys, and adrenals, including anatomical details, better on 2D IP/OP images than on 3D IP/OP images ($P<0.001$).

Image artefacts Both readers found more motion artefacts (blurring as well as ghosting) on 3D IP/OP images than on 2D IP/OP images (both, $P<0.001$) (Fig. 3). The extent of Gibbs ringing, parallel imaging, and susceptibility artefacts on 3D vs. 2D IP/OP images was not rated differently by either reader ($P=0.061$-0.297). Larger extents of inflow and vascular ghosting artefacts were present on 2D IP/OP as opposed to 3D IP/OP images by both readers ($P<0.001$).

Table 1 Comparison of 2D versus 3D in- and out-of-phase imaging in regard to anatomic conspicuity, imaging artefacts, and overall image quality

	Reader 1		2D vs. 3D (*P*-value)	Reader 2		2D vs. 3D (*P* -value)
	2D	3D		2D	3D	
Conspicuity (%)						
Liver	83/227 (37 %)	16/227 (7 %)	<0.001*	78/227 (34 %)	16/227 (7 %)	<0.001*
Kidney	91/227 (40 %)	8/227 (4 %)	<0.001*	88/227 (39 %)	15/227 (7 %)	<0.001*
Adrenals	97/227 (43 %)	19/227 (8 %)	<0.001*	72/227 (32 %)	7/227 (3 %)	<0.001*
Artefacts (%)						
Motion ghosting	91/227 (40 %)	142/227 (63 %)	<0.001*	99/227 (44 %)	148/227 (65 %)	<0.001*
Motion blurring	71/227 (31 %)	137/227 (60 %)	<0.001*	35/227 (15 %)	128/227 (56 %)	<0.001*
Gibbs ringing	28/227 (12 %)	36/227 (16 %)	=0.157	21/227 (9 %)	27/227 (12 %)	=0.257
Parallel imaging	49/227 (22 %)	42/227 (19 %)	=0.297	48/227 (21 %)	30/227 (13 %)	=0.055
Vascular ghosting	71/227 (31 %)	30/227 (13 %)	<0.001*	56/227 (25 %)	39/227 (17 %)	<0.001*
Inflow	224/227 (99 %)	13/227 (6 %)	<0.001*	220/227 (97 %)	10/227 (4 %)	<0.001*
Susceptibility	81/227 (36 %)	78/227 (34 %)	=0.196	52/227 (23 %)	40/227 (18 %)	=0.061
Image quality	4.03±0.75	3.47±0.85	<0.001*	3.96±0.50	3.76±0.73	<0.001*

For anatomic conspicuity and imaging artefacts, percentages of superior 3D or 2D image series are displayed. For image quality the mean including standard deviation of the overall rating of both readers is displayed (scale 1–5 with 5 being the best possible image quality). *Significant differences

Overall image quality Image quality of all 2D and 3D IP/OP images was rated diagnostic by both readers. Reader 1 (R1) and reader 2 (R2) rated the image quality in 80.2 % and 86.8 % of IP and OP images as good or excellent, but only in 50.2 % and 69.2 % of 3D IP and OP images. In 55.1 % and 21.6 % of cases, the image quality of 2D images was rated higher than that of 3D images, whereas the quality of 3D images was rated higher than that of 2D images in 5.0 % and 6.0 % of cases.

Detection of liver lesions Overall, both readers (R1/R2) detected significantly more liver lesions on 2D IP/OP images (525/501) than on 3D IP/OP images (492/488) in all 227 patients (P=0.003/0.001). Conversely, no significant difference was seen between the two readers (R1 and R2) for detection of fat-containing liver lesions on 2D IP/OP images (49/46) and on 3D IP/OP images (44/44) in all 227 patients (P=0.334/0.317) (Fig. 2).

Quantitative assessment of LFC In both liver lobes (segments II and VIII) 3D $FSF_{IP/OP}$ was slightly but significantly higher than 2D $FSF_{IP/OP}$ (P=0.051/0.033), with a small mean bias of +0.28 % and +0.46 % respectively. Moreover, FSF_{FAT} was significantly higher than both 3D $FSF_{IP/OP}$ and 2D $FSF_{IP/OP}$ (all $P<0.001$) with a mean bias of +2.46 % and +2.88 % as well as +3.25 % and +3.43 % respectively (Table 2, Fig. 4).

Duration of 3D and 2D SPGR-DE sequences Mean imaging time of 3D and 2D SPGR-DE was 23.7±2.9 and 97.2±9.1 s. No significant correlation was found between imaging time and image quality of 3D SPGR-DE for both readers with a Pearson correlation coefficient of 0.075 and -0.028 respectively (P=0.258; P=0.672).

Discussion

The rationale behind this study was to determine whether or not we could replace our multiple-breath-hold 2D IP/OP dual gradient-echo acquisition by a single-breath-hold 3D dual gradient-echo sequence with fat and water separation,

Table 2 Qualitative assessment of liver fat content (LFC) in patients without diffuse liver disease (n=139)

LFC quantification (fat index; %)	2D IP/OP	3D IP/OP	Fat-only
Segment II	6.2±5.1 (0.1–32.4)	6.7±5.2 (0.1–33.6)	9.6±5.2 (1.0–33.9)
Segment VIII	6.0±5.3 (0.1–32.3)	6.3±5.5 (0.1–32.7)	9.3±5.1 (1.6–32.7)

One blinded reader determined the fat index (%) by placing regions of interest in liver segment II and VIII on computed fat signal fraction maps derived from 2D and 3D in-/out-of-phase (IP/OP) as well as fat-/water-signal only images (fat-only)

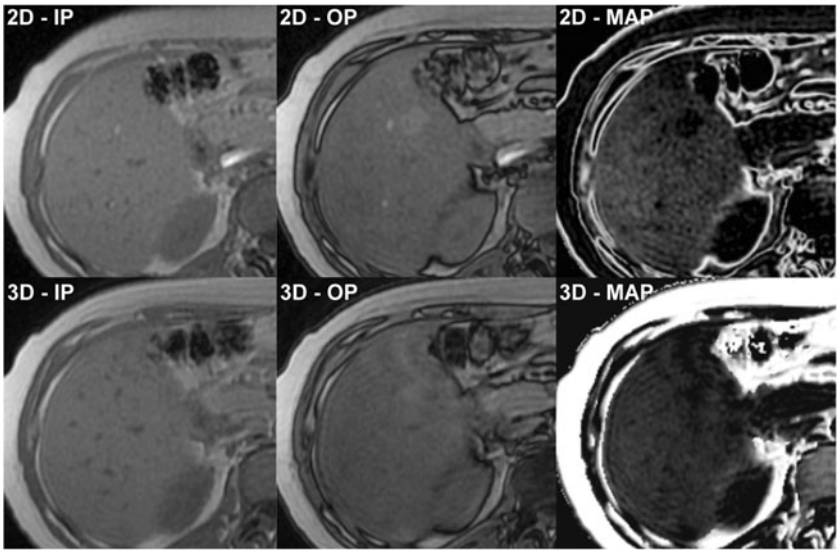

Fig. 3 Axial 2D and 3D IP/OP images with corresponding fat fraction maps of a 25-year-old patient undergoing liver MRI because of an unclear hyperechogenic liver lesion. The 2D images clearly depict the lesion in liver segment V allowing for diagnosis of focal fatty sparing in hepatic steatosis. On 3D images the lesion was missed, hypothetically predominantly because of breathing artefacts (motion ghosting) resulting in lower image quality as compared to the 2D images and because of the slightly different weighting of image contrast. Both 2D and 3D images allowed detection of surrounding liver steatosis based on the characteristically lower signal intensity in OP images in comparison to IP images and by elevated signal on the fat fraction maps

which possibly could also serve as an unenhanced baseline acquisition for subsequent dynamic contrast-enhanced fat-supressed imaging. If we could do so, our total liver protocol would be shorter and more time efficient.

Imaging sequences

Two-dimensional SPGR-DE is commonly used and well established for IP/OP evaluation of liver steatosis as well as fatty liver lesions in clinical routine [7]. Sufficient SNR and substantial T1 weighting are achieved by relatively long TR times and high excitation flip angles. The MR software typically allows splitting of the acquisition into several breath-hold periods, whose duration can be adapted easily and flexibly to the capacity of a patient to hold the breath. Motion artefacts are often restricted to few images only.

The recently developed 3D SPGR-DE sequence has already been recommended for replacement of 2D SPGR-DE [17]. It offers the advantages of acquisition of contiguous and thinner slices with whole-liver coverage in a single breath-hold [18], allowing for a fast assessment of hepatic steatosis comparable to fat-selective imaging methods [19]. The faster acquisition times of 3D SPGR-DE are realised by technical advances in parallel imaging and a shortening of TR times, with concomitant reduction of excitation flip angles, which is beneficial when profiting from the inherent SNR advantage of a 3D versus 2D sequence. On the downside, any motion during the breath-hold period will lower the image quality of all images in the 3D acquisition. A splitting of the acquisition into a shorter breath-hold period would annihilate the advantages of a 3D acquisition and cannot be conveniently implemented in the MR system software. Such a splitting would also not be helpful when using the sequence for dynamic imaging, particularly the transient arterial phase. Thus, we resorted to adjusting the encoded matrix size, comparable to the single-echo 3D-GRE basic sequence, which we would like to replace in addition to the 2D SPGR-DE sequence.

Image quality

Previous studies found fat-suppressed single-echo 3D-GRE sequences to yield liver images of comparable quality to those obtained with standard 2D-GRE sequences [20], and 2D and 3D dual-echo gradient-echo sequences were shown equally suitable for characterisation of adrenal lesions at 3 T [21]. However, our results suggested that 3D SPGR-DE was more susceptible to artefacts, especially caused by patient motion. One reason for the higher amount of motion blurring and motion ghosting artefacts of 3D SPGR-DE in our study could be the significantly longer acquisition times of SPGR-DE compared to single-echo 3D-GRE [22] because of the longer TR necessary to capture two echoes. Whereas 3D SPGR-DE is fast enough for imaging of the adrenals, liver imaging in our study required an average breath-hold capability of 24±3 s, which seems critical for patients with reduced breath-hold capabilities.

Moreover, compared with single-echo 3D-GRE, 3D SPGR-DE lacks spectrally selective radiofrequency-based fat suppression, which can reduce motion artefacts in T1-

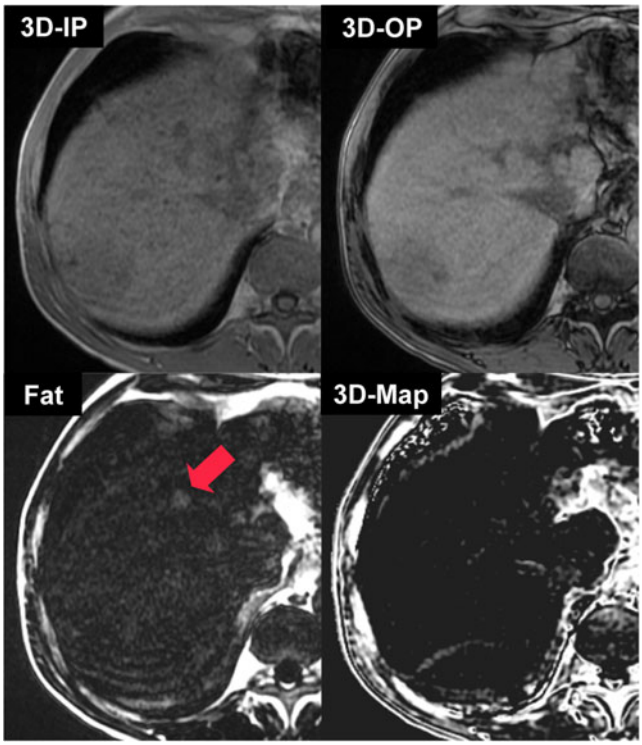

Fig. 4 Axial 3D IP/OP images with automatic reconstruction of fat-only images and corresponding 3D IP/OP fat fraction maps of a 56-year-old patient suffering from liver cirrhosis (Child B) with biopsy-proven moderate-to-severe iron overload of liver parenchyma. In contrast to fatty infiltration of the liver, iron deposition causes an accelerated signal decay resulting in a significant signal drop from OP to IP images due to the typically shorter echo time of the OP than of the IP acquisition at 1.5 T. Fat-only images show a false-positive fatty infiltration of the liver (hyperintense signal) as well as a focal fatty liver lesion (arrow) caused by the image reconstruction algorithm, whereas 3D IP/OP fat fraction maps, derived with the constraint $SI_{OP} \geq SI_{IP}$, correctly yield a liver fat content of 0 %

weighted images [22]. By comparison, multiple-breath-hold 2D SPGR showed significantly better image quality, especially in patients with reduced breath-hold capabilities. However, the higher robustness of the 2D SPGR-DE as compared to the single breath-hold 3D SPGR sequence used in our study is achieved by splitting the MR acquisition volume into two to three breath-hold periods of 14 s each, resulting in an almost four times longer imaging time (97.2 ±9.1 s versus 23.7±2.9).

Consistent with a prior study [20] we found the visualisation and depiction of the abdominal anatomy to be of lower quality in 3D than in 2D dual-echo images. The quality of 2D images was rated higher than that of 3D images in approximately a third of patients. However, similar to 2D SPGR-DE, the overall image quality of the 3D images was rated as being diagnostic in all 227 patients.

Interestingly, motion artefacts as well as the quality of the 3D images did not correlate with the acquisition time of the 3D sequence. We hypothesise that this is because the MR parameters were adapted to the single-echo 3D-GRE baseline acquisition resulting in longer acquisition times/breath-hold times (mean 4 s), which was only tolerated by patients with good ability to suspend respiration.

Whereas both techniques resulted in similar amounts of parallel imaging, susceptibility, or ringing artefacts, 3D SPGR-DE produced a significantly lower amount of inflow and vascular ghosting artefacts, which, however, seemed to be of minor importance for overall image quality.

Detection of liver fat

Regarding the clinically relevant evaluation of focal and diffuse liver fat, no significant difference was seen in this study between the two IP/OP techniques for depiction of focal fatty liver lesions, although the detection rate for liver lesions of any kind was lower in 3D than in 2D images. The discrepancy in the results for detection of all liver lesions versus fat-containing liver lesions might be due to the short repetition time and the small flip angle of the 3D sequence, which result in an increased T1 weighting of the image contrast and therefore possibly a higher sensitivity to low lipid contents as compared to 2D SPGR [21]. However, IP/OP imaging is used for characterisation rather than detection of liver lesions, putting into perspective the inferior results in detection of liver lesions of any kind by evaluation of the 3D sequence.

The difference in the imaging parameters might also partly explain the slightly but significantly higher quantitative estimation of LFC in both liver lobes determined from 3D images as compared to 2D images. However, both techniques have been shown to yield accurate quantification of LFC in comparison to histopathology before [23–25]. Thus, these small differences may be of little relevance for clinical routine.

Compared with the equivalent LFC estimations based on 2D and 3D IP/OP images, those based on fat-only images, which were shown to ease image interpretation when available along with the IP/OP images [24], were significantly higher when compared to LFCs from both 2D and 3D IP/OP. Detailed analysis of our data suggests that the discrepancies between fat-only and IP/OP-based quantifications were particularly large for low fat signal fractions. These differences are consistent with previously published studies showing an overestimation of low fat contents in fat-signal-only images based on two-point Dixon raw data [24, 26] and are most probably explained by noise-related bias present in fat-only images [27], which affects the separation of water and fat signals [27].

Finally, an additional factor contributing to the discrepant fat-content estimations based on fat-only images may have been the application of a B1 inhomogeneity correction of the images ("PURE" filter), which increased the noise in central body regions far from the surface receiver coil and let dark central fat-free liver lesions appear brighter.

Accordingly single-breath-hold 3D SPGR-DE performs as well as multiple-breath-hold 2D SPGR-DE for the qualitative and quantitative assessment of liver fat. However on the basis of our technical results, we recommend the use of 2D SPGR-DE in patients showing restricted breath-hold capabilities because of improvements in image quality.

We have to acknowledge the following study limitations concerning the quantification of LFC. First, the 2D and 3D SPGR-DE sequence and reconstruction algorithm used did not address T1 and T2* relaxation effects that confound chemical shift imaging. Accordingly we excluded patients with diffuse liver disease from the quantitative analysis as previous studies indicate that T2* bias might be neglectable for accurate liver fat quantification in patients without elevated hepatic iron [7–10]. In comparison, newly proposed multi-echo sequences are able to correct for T2*-bias caused by coexisting liver iron overload and might have yielded more accurate estimates of LFC. Drawbacks of ME-MRI include longer imaging times and lower spatial resolution respectively as compared to DE-MRI [28], which might diminish detection of focal fatty infiltration or characterisation of focal liver lesions in clinical routine.

Secondly, there was no gold standard for liver fat quantification available. Thus, while the evaluation of fat-signal-only images may have led to false-positive diagnoses of steatosis, the evaluation of IP/OP images may have caused false-negative diagnoses. However, the aim of our study was to evaluate differences between 2D and 3D SPGR-DE in a clinical setting, and the accuracy of LFC quantification was probed for both sequences in other earlier studies [23–25].

In conclusion, our study indicates that single-breath-hold 3D SPGR-DE can replace multiple-breath-hold 2D SPGR-DE for the assessment of focal and diffuse fatty infiltration of liver parenchyma. The MR acquisition time for the 3D SPGR-DE was shorter than for 2D SPGR-DE, but was more susceptible to breathing artefacts, resulting in a lower image quality in patients with reduced breath-hold capabilities. Finally, evaluations of 3D fat-only images yielded small but significantly higher LFC estimations than those based on IP/OP images.

References

1. Schwimmer JB, Deutsch R, Kahen T, Lavine JE, Stanley C, Behling C (2006) Prevalence of fatty liver in children and adolescents. Pediatrics 118:1388–1393
2. Falck-Ytter Y, Younossi ZM, Marchesini G, McCullough AJ (2001) Clinical features and natural history of nonalcoholic steatosis syndromes. Semin Liver Dis 21:17–26
3. Clavien PA, Petrowsky H, DeOliveira ML, Graf R (2007) Strategies for safer liver surgery and partial liver transplantation. N Engl J Med 356:1545–1559
4. Cassidy FH, Yokoo T, Aganovic L et al (2009) Fatty liver disease: MR imaging techniques for the detection and quantification of liver steatosis. Radiographics 29:231–260
5. Hines CD, Yu H, Shimakawa A et al (2010) Quantification of hepatic steatosis with 3-T MR imaging: validation in ob/ob mice. Radiology 254:119–128
6. Raptis DA, Fischer MA, Graf R et al (2012) MRI: the new reference standard in quantifying hepatic steatosis? Gut 61:117–127
7. d'Assignies G, Kauffmann C, Boulanger Y et al (2011) Simultaneous assessment of liver volume and whole liver fat content: a step towards one-stop shop preoperative MRI protocol. Eur Radiol 21:301–309
8. d'Assignies G, Ruel M, Khiat A et al (2009) Noninvasive quantitation of human liver steatosis using magnetic resonance and bioassay methods. Eur Radiol 19:2033–2040
9. Kim H, Taksali SE, Dufour S et al (2008) Comparative MR study of hepatic fat quantification using single-voxel proton spectroscopy, two-point dixon and three-point IDEAL. Magn Reson Med 59:521–527
10. Westphalen AC, Qayyum A, Yeh BM et al (2007) Liver fat: effect of hepatic iron deposition on evaluation with opposed-phase MR imaging. Radiology 242:450–455
11. Reeder SB, Cruite I, Hamilton G, Sirlin CB (2011) Quantitative assessment of liver fat with magnetic resonance imaging and spectroscopy. J Magn Reson Imaging 34:729–749
12. Hines CD, Frydrychowicz A, Hamilton G et al (2011) T(1) independent, T(2) (*) corrected chemical shift based fat-water separation with multi-peak fat spectral modeling is an accurate and precise measure of hepatic steatosis. J Magn Reson Imaging 33:873–881
13. Kohgo Y, Ohtake T, Ikuta K, Suzuki Y, Torimoto Y, Kato J (2008) Dysregulation of systemic iron metabolism in alcoholic liver diseases. J Gastroenterol Hepatol 23(Suppl 1):S78–S81
14. Ma J, Vu AT, Son JB, Choi H, Hazle JD (2006) Fat-suppressed three-dimensional dual echo Dixon technique for contrast agent enhanced MRI. J Magn Reson Imaging 23:36–41
15. Ma J (2004) Breath-hold water and fat imaging using a dual-echo two-point Dixon technique with an efficient and robust phase-correction algorithm. Magn Reson Med 52:415–419
16. Mason D (2009) pydicom: a pure python package for working with DICOM files. http://pypi.python.org/pypi/pydicom/. Accessed 14.03.2011.
17. Ringe KI, Husarik DB, Sirlin CB, Merkle EM (2010) Gadoxetate disodium-enhanced MRI of the liver: part 1, protocol optimization and lesion appearance in the noncirrhotic liver. AJR Am J Roentgenol 195:13–28
18. Rofsky NM, Lee VS, Laub G et al (1999) Abdominal MR imaging with a volumetric interpolated breath-hold examination. Radiology 212:876–884
19. Springer F, Ehehalt S, Sommer J et al (2011) Assessment of relevant hepatic steatosis in obese adolescents by rapid fat-selective GRE imaging with spatial-spectral excitation: a quantitative comparison with spectroscopic findings. Eur Radiol 21:816–822
20. Kim MJ, Mitchell DG, Ito K, Kim PN (2001) Hepatic MR imaging: comparison of 2D and 3D gradient echo techniques. Abdom Imaging 26:269–276
21. Marin D, Soher BJ, Dale BM, Boll DT, Youngblood RS, Merkle EM (2010) Characterization of adrenal lesions: comparison of 2D and 3D dual gradient-echo MR imaging at 3T–preliminary results. Radiology 254:179–187
22. Mitchell DG, Vinitski S, Saponaro S, Tasciyan T, Burk DL, Rifkin MD Jr (1991) Liver and pancreas: improved spin-echo T1 contrast by shorter echo time and fat suppression at 1.5 T. Radiology 178:67–71
23. Cesbron-Metivier E, Roullier V, Boursier J et al (2010) Noninvasive liver steatosis quantification using MRI techniques combined with blood markers. Eur J Gastroenterol Hepatol 22:973–982

24. Fischer MA, Nanz D, Reiner CS et al (2010) Diagnostic performance and accuracy of 3-D spoiled gradient-dual-echo MRI with water- and fat-signal separation in liver-fat quantification: comparison to liver biopsy. Invest Radiol 45:465–470
25. McPherson S, Jonsson JR, Cowin GJ et al (2009) Magnetic resonance imaging and spectroscopy accurately estimate the severity of steatosis provided the stage of fibrosis is considered. J Hepatol 51:389–397
26. Boll DT, Marin D, Redmon GM, Zink SI, Merkle EM (2010) Pilot study assessing differentiation of steatosis hepatis, hepatic iron overload, and combined disease using two-point dixon MRI at 3T: in vitro and in vivo results of a 2D decomposition technique. AJR Am J Roentgenol 194:964–971
27. Liu CY, McKenzie CA, Yu H, Brittain JH, Reeder SB (2007) Fat quantification with IDEAL gradient echo imaging: correction of bias from T(1) and noise. Magn Reson Med 58:354–364
28. Meisamy S, Hines CD, Hamilton G et al (2011) Quantification of hepatic steatosis with T1-independent, T2-corrected MR imaging with spectral modeling of fat: blinded comparison with MR spectroscopy. Radiology 258:767–775